

# Noninvasive Multiplexed Analysis of Bladder Cancer-Derived Urine Exosomes via Janus Magnetic Microspheres

Xiaowei Wei, Lijun Cai, Hanxu Chen, Luoran Shang,\* Yuanjin Zhao,\* and Weijian Sun\*



Cite This: *Anal. Chem.* 2022, 94, 18034–18041



Read Online

ACCESS |



Metrics & More



Article Recommendations



Supporting Information



**ABSTRACT:** Bladder cancer greatly endangers human health, and its early diagnosis is of vital importance. Exosomes, which contain proteins and nucleic acids related to their source cells, are expected to be an emerging biomarker for bladder cancer detection. Here, we propose a novel system for multiplexed analysis of bladder cancer-derived urine exosomes based on Janus magnetic microspheres as barcoded microcarriers. The microcarriers are constructed by droplet-templated coassembly of colloidal silica nanoparticles and magnetic nanoparticles under a magnetic field. The microcarriers possess one hemisphere with structural color and the other hemisphere with magneto-responsiveness. Benefiting from the unique structure, these Janus microcarriers could serve as barcodes and could move controllably in a sample solution, thus realizing the multiplex detection of exosomes with high sensitivity. Notably, the present platform is noninvasive since a urine specimen, as an ideal source of bladder cancer-derived exosomes, is employed as the sample solution. This feature, together with the good sensitivity, specificity, low sample consumption, and easy operation, indicates the great potential of the platform for bladder cancer diagnosis in clinical applications.

## 1. INTRODUCTION

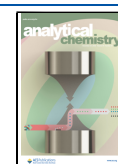
Bladder cancer is one of the most popular malignant tumors of the urinary system with both incidence rate and mortality maintaining an upward trend.<sup>1–3</sup> There are currently plenty of methods for initial diagnosis of bladder cancer, including cystoscopy, exfoliation cytology, tumor marker detection, etc.<sup>4–6</sup> In particular, tumor marker analysis has aroused great concern for its better patient compliance and high sensitivity.<sup>7–12</sup> Among various tumor markers, exosomes are promising indicators for the diagnosis of bladder cancer.<sup>13–18</sup> Exosomes are extracellular vesicles that carry nucleic acids, proteins, and lipids associated with their mother cells. Analysis on cancer-related exosomes could provide tumorigenesis information as well as clinical implications.<sup>19–22</sup> However, current methods for exosome detection often require collection of tissue specimens or blood samples, which is invasive and could cause discomfort to patients. Besides, conventional analytical platforms can only identify a single type of exosome,<sup>23,24</sup> while multiplex analysis of exosomes derived from different cells remains elusive. These drawbacks, together with the requirement of bulk instruments and demanding operations,<sup>25–28</sup> hinder us from getting sufficient tumorigenesis information regarding exosomes. Therefore, a novel non-invasive and multiplex analysis platform for diagnosis and monitoring of bladder cancer is highly anticipated.

Herein, we propose a multiplex assay platform based on Janus magnetic photonic crystal (PhC) microsphere barcodes for noninvasive analysis of bladder cancer-derived urine exosomes, as shown in Figure 1. Barcodes are molecular tags or particles that carry distinguishable information for encoding and identification. Specifically, PhCs stand out as powerful barcodes due to their distinctive structural color signatures derived from their periodically ordered microstructures.<sup>25</sup> Benefiting from the stable and accurate optical coding ability, PhC barcodes have been applied in multiplex analysis of various biological samples including biomacromolecules, cells, and microbes. However, the application of classical PhC barcodes in detecting trace biomarkers in urine is limited because of unsatisfactory sensitivity resulting from insufficient contact between the barcodes and the biomarkers. In contrast, Janus magnetic particles possess a compartmentalized structure with one half susceptible to magnetic fields and are thus capable of controllable motion and rotation, as well as

**Received:** October 7, 2022

**Accepted:** December 6, 2022

**Published:** December 15, 2022



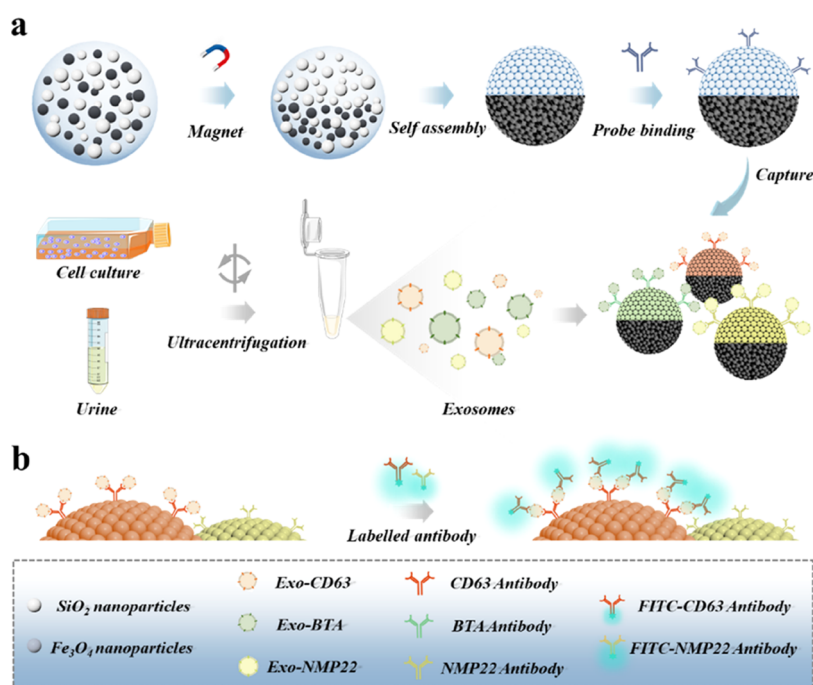


**Figure 1.** Schematic diagram of the Janus magnetic microspheres for noninvasive analysis of bladder cancer-derived urinary exosomes. (a) Preparation of the Janus magnetic microspheres and the immobilization of antibody probes for exosome identification and capture and (b) multiplex exosome analysis platform based on the Janus magnetic microsphere barcodes.

enrichment and separation of analytes.<sup>29,30</sup> It is thus conceived that, by composing PhC barcodes with Janus magnetic property, a novel multiplex assay platform could be constructed for noninvasive analysis of trace biomarkers in urine.

In this paper, we prepared Janus magnetic PhC microspheres by droplet microfluidics and magnetic-induced phase separation. The microspheres exhibited a Janus structure with one half showing characteristic structural colors of as encoding elements and the other half endowed with magneto-responsiveness. The structural color of the microspheres enabled barcoded analysis of exosomes, while the magneto-responsiveness feature contributed to the controllable rotation of the microspheres in the sample solution, thereby improving the detection sensitivity and enrichment efficiency. Based on this, a multiplex exosome analysis platform was established, and the capability of identifying different types of exosomes in a single test was validated. Besides, noninvasive analysis of urinary exosomes from bladder cancer cells has been realized, which manifested high sensitivity and specificity. Moreover, dynamic monitoring of the expression of exosome markers was accomplished. The implication of these results is that the Janus magnetic microspheres are ideal barcodes in noninvasive exosome analysis, and the associated multiplex bioassay platform has great potential for clinical diagnosis of bladder cancer.

## 2. EXPERIMENTAL SECTION

**2.1. Materials.** 2-Mercapto ethanol sulfonic acid (MES), 1-(3-dimethylaminopropyl)-3-ethylcarbodiimide hydrochloride (EDC), and *n*-hydroxy succinimide (NHS) were derived from Sigma-Aldrich (Shanghai, China). Ferric chloride ( $\text{FeCl}_3$ ) and ferrous chloride ( $\text{FeCl}_2$ ) were obtained from Aladdin (Shanghai, China). Anti-CD63 antibody, anti-bladder tumor-associated antigen (BTA) antibody, anti-NMP22 antibody, and

the corresponding fluorescein isothiocyanate (FITC)-labeled antibodies were purchased from Abcam. High-glucose Dulbecco's modified Eagle medium (DMEM), F12K medium, and fetal bovine serum (FBS, exosome removal) were derived from Hyclone (UT). Penicillin–streptomycin solution was purchased from Gibco. Uranium acetate was derived from Yi he biotechnology Co., Ltd. (Shanghai, China). The cell lines used were obtained from the Cell Bank of Chinese Academy of Sciences (Shanghai, China). Methyl silicone oil was purchased from Shin-etsu (Japan). All deionized water used in the experiments was purified by Millipore (Bedford). All buffer solutions were prepared with deionized water. All chemicals were of optimum grade available and used according to the specifications. The microfluidics constant pressure pump and the mechanical injection pump were derived by Microfluidic Technology Co., Ltd. (Suzhou, China). The clinical specimens were collected from the Second Affiliated Hospital of Nanjing Medical University in accordance with China's urine collection standard technique (Table S1) and the guidelines issued by the Ethics Committee of the Chinese Academy of Sciences.

**2.2. Preparation of Silica Nanoparticles and  $\text{Fe}_3\text{O}_4$  Nanoparticles.** The Stöber method was used to synthesize the silica nanoparticles.<sup>31</sup> After repeated centrifugation and purification, silica nanoparticles with uniform size were obtained. The dispersion of silica nanoparticles was prepared by adding deionized water, and the nanoparticles were dispersed evenly by ultrasonic treatment.  $\text{Fe}_3\text{O}_4$  nanoparticles were prepared by coprecipitation of ferric chloride and ferrous chloride.<sup>32</sup> The resultant magnetic nanoparticles were purified by repeated magnetic precipitation and washing. Finally, the silica nanoparticle dispersion (20% W/V) was mixed with the magnetic nanoparticle dispersion (20% W/V), and the prepared mixture was ready for use after ultrasonic oscillation.

**2.3. Preparation of Janus Magnetic Microspheres.** Janus magnetic microspheres were prepared through droplet

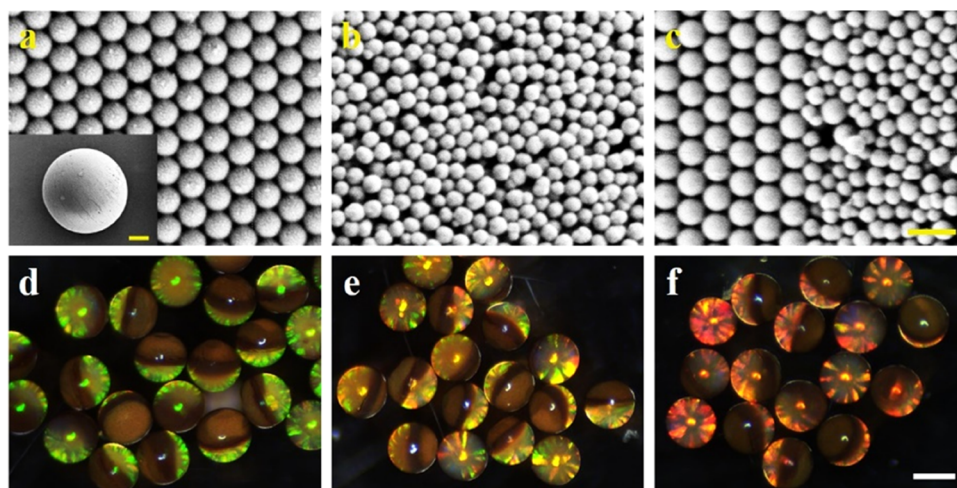


**Figure 2.** (a–c) SEM images of (a) the surface of the silica colloidal crystal hemisphere, (b) the surface of the magnetic hemisphere, and (c) the boundary between the colloidal crystal hemisphere and the magnetic hemisphere of the Janus magnetic microsphere. The scale bar is 400 nm. The inset image in panel (a) is an intact Janus magnetic microsphere. The scale bar is 50  $\mu\text{m}$ . (d–f) Three groups of Janus magnetic microspheres with (d) bright green, (e) yellow-green, and (f) orange-red structural colors. The scale bar is 200  $\mu\text{m}$ .

microfluidic technology.<sup>33–36</sup> Briefly, silicon oil (50 cSt) was utilized as the continuous phase, and the aqueous suspension of silica and  $\text{Fe}_3\text{O}_4$  nanoparticles was used as the dispersed phase. Droplets were generated and collected in the high-viscosity silicon oil (500 cSt) and then placed in an oven to evaporate the solvent, during which a magnet was applied to induce phase separation inside the droplet. Janus magnetic microspheres were obtained after 12 h, underwent repeated washing by *n*-hexane, and finally calcined in a Muffle furnace at 800  $^\circ\text{C}$ .

**2.4. Cell Culture and Exosome Extraction.** Human bladder cancer cell line T24 was cultured in high-glucose DMEM medium containing 10% exosome-free fetal bovine serum (FBS), 1% penicillin–streptomycin at 37  $^\circ\text{C}$  with 5%  $\text{CO}_2$  supply, while human bladder epithelial immortal cells Sv-huc-1 were cultured in the F12K medium, similarly. The culture supernatant was collected after 2–3 days of culture, and the exosomes were isolated by ultracentrifugation. Both cell lines were cultured three times under the same conditions, and the independent supernatant samples were collected. The supernatant was taken and centrifuged at 300g at 4  $^\circ\text{C}$  for 10 min. The supernatant was collected and centrifuged at 2000g for 10 min to remove the dead cells. Then, the obtained supernatant was centrifuged at 10,000g for 10 min to remove the cell debris. The final supernatant was ultracentrifuged at 140,000g for 70 min to precipitate and collect the exosomes. These pellets were washed with phosphate-buffered saline (PBS) buffer solution, and the mixed contaminants were removed by 0.22  $\mu\text{m}$  filter and centrifuged again at 140,000g superspeed for 70 min. Lastly, the exosomes were suspended in 100  $\mu\text{L}$  of PBS buffer at  $-80\text{ }^\circ\text{C}$  for the subsequent application. Western blot was used to detect the exosome characteristic protein CD63 and the bladder cancer-related markers BTA and NMP22. The particle size distribution and the exosome concentration in the suspension were measured by nanoparticle tracking analysis (NTA).

**2.5. Exosome Analysis Using Janus Magnetic Microspheres.** **2.5.1. Probe Molecule Coupling.** Janus magnetic microspheres were aminated by APTES, followed by succinic anhydride carboxylation. In MES solution (pH 5.9), carboxyl

groups were activated by NHS and EDC to conjugate with the antibodies in the exosomes.

**2.5.2. Exosome Capture.** Janus magnetic microspheres with probe antibody immobilized were sealed in bovine serum albumin (BSA) solution. The microspheres were then transferred to the exosome solution and then incubated at 37  $^\circ\text{C}$  for 6 h to make the antibody probes react fully with the exosome markers CD63, NMP22, and BTA. Finally, PBS buffer was used to wash the microspheres three times to remove the untargeted exosomes.

**2.5.3. Detection of Exosome Markers.** In the detection platform, fluorescence-labeled antibodies were added to react with the exosome markers. The Janus magnetic microspheres were washed three times with PBS buffer to avoid the interference of the fluorescence signal caused by nonspecific adsorption. The fluorescence signal was used to decode the multiplexed analysis results. Clinical urine specimens were collected in 50 mL centrifuge tubes, and then, they were centrifuged at a speed of 2000 rpm for 10 min to remove cells. The liquid supernatant was collected in new centrifuge tubes (50 mL) for later analysis. The Janus barcodes with different characteristic reflection wavelengths were utilized for the multiple encoding of exosomal biomarkers during the fluorescence intensity measurement for the quantitative analysis.

**2.6. Characterization.** The morphology of exosomes was identified using a scanning electron microscope (SEM, s-300n, Hitachi) and a transmission electron microscope (TEM, HT7700, Hitachi). A charge coupled device (CCD, Olympus, DP30BW) was used for the optical imaging of Janus barcodes, while the microstructure was characterized using a scanning electron microscope (S-300N, Hitachi, Japan). The reflectivity peaks of Janus barcodes were measured using a fiber optic spectrometer (Marine Optics, USB2000+). Exosome markers were detected using a stereoscopic microscope (Olympus, BX53) and a CCD camera, and multiplexed analysis of the microspheres was performed. Besides, the fluorescence intensity was quantified using a fluorescence microscope (Olympus, CKX41) coupled with a fiber optic spectrometer (Ocean Optics, HR2000).



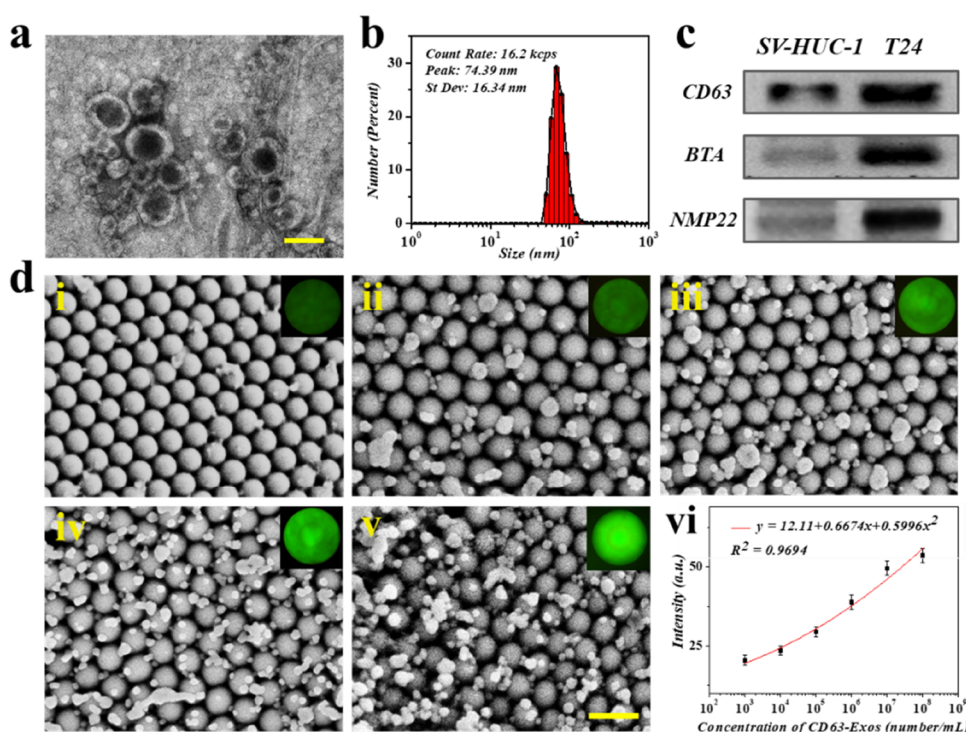


**Figure 3.** (a) Microscopic characterization of bladder cancer exosomes by TEM. The scale bar is 100 nm; (b) particle size analysis of bladder cancer exosomes; (c) Western blot analysis of exosome markers; (d) (i–v) representative SEM images showing the capture of different concentrations of bladder cancer CD63 exosomes by the Janus magnetic microspheres. The scale bar is 200 nm; (vi) corresponding plot of fluorescence intensity as a function of exosome concentration. Insets in (i–v) are the fluorescence microscopic image of a microsphere. The error bars in panel (vi) are the standard deviation of three repeated experiments.

### 3. RESULTS AND DISCUSSION

**3.1. Preparation and Characterization of Janus Magnetic Microspheres.** In a typical preparation experiment, Janus magnetic microspheres were generated through microfluidic technology integrated with magnetic induction.<sup>37–41</sup> Droplet templates were first prepared by microfluidic emulsification using an aqueous suspension of SiO<sub>2</sub> nanoparticles and Fe<sub>3</sub>O<sub>4</sub> nanoparticles as the dispersed phase while silicon oil as the continuous phase (Figure S1). With the subsequent evaporation process, the SiO<sub>2</sub> nanoparticles in the droplets gradually self-assembled and formed periodic arrays. At the same time, a magnet was placed to induce phase separation within the droplet. As a result, the Fe<sub>3</sub>O<sub>4</sub> nanoparticles deposited to the bottom of the droplet, thereby generating Janus microspheres. The two hemispheres of the Janus particle with different distribution of the nanoparticles were verified by scanning electron microscopy (SEM) and element analysis (Figure S2). Due to the participation of the magnetic nanoparticles, these microspheres could be induced by an external magnetic field for rotational or directional motion, as shown in Figures S3–S5. The microstructure of the Janus microspheres was characterized by SEM. We found that SiO<sub>2</sub> nanoparticles exhibited an orderly hexagonal close packing structure in one hemisphere (Figure 2a), while they were disorderly arranged in the other hemisphere with interstices filled with smaller Fe<sub>3</sub>O<sub>4</sub> nanoparticles (Figures 2b and S6). In addition, the boundary between the two hemispheres is clearly displayed in Figure 2c.

We next investigated the optical encoding ability of the Janus magnetic microspheres. We found that one hemisphere of the Janus microspheres exhibited bright color. This was

attributed to the periodically ordered silica nanoparticles, which formed a typical colloidal crystal structure and gave rise to a photonic bandgap. Such a unique phenomenon was manifested by the characteristic reflection spectrum, and the peak wavelength was calculated in accordance with the Bragg diffraction formula<sup>42–45</sup>

$$\lambda = 1.633dn_{\text{average}} \quad (1)$$

where  $\lambda$  represents the wavelength of the reflection peak,  $d$  represents the distance between the center of two adjacent spherical silica nanoparticles, and  $n_{\text{average}}$  is the average refractive index. Once the composition of the microcarriers is selected,  $n_{\text{average}}$  is constant. Therefore, using silica nanoparticles of different sizes, we obtained multifarious Janus magnetic microspheres with bright green, yellow-green, and orange-red structural colors (Figure 2d–f). The corresponding reflection spectra of these Janus magnetic microspheres are shown in Figure S7a with the reflection peaks at 565, 595, and 610 nm, respectively. The adjustable structural color of the Janus magnetic microspheres set a technical basis for multiplexed encoding. Besides, considering the anisotropic geometry of the Janus magnetic nanospheres, we measured their reflection spectrum under different angles of rotation. We found that the reflection peak position remained unchanged although the intensity gradually decreased when the microspheres rotated away from the incident light (Figure S7b). This indicated that the Janus magnetic microspheres could maintain a stable optical readout regardless of their positions or rotations, which was favorable for subsequent bioanalysis studies.

**3.2. Extraction of Bladder Cancer Exosomes.** We then explored the capability of the Janus magnetic microspheres for



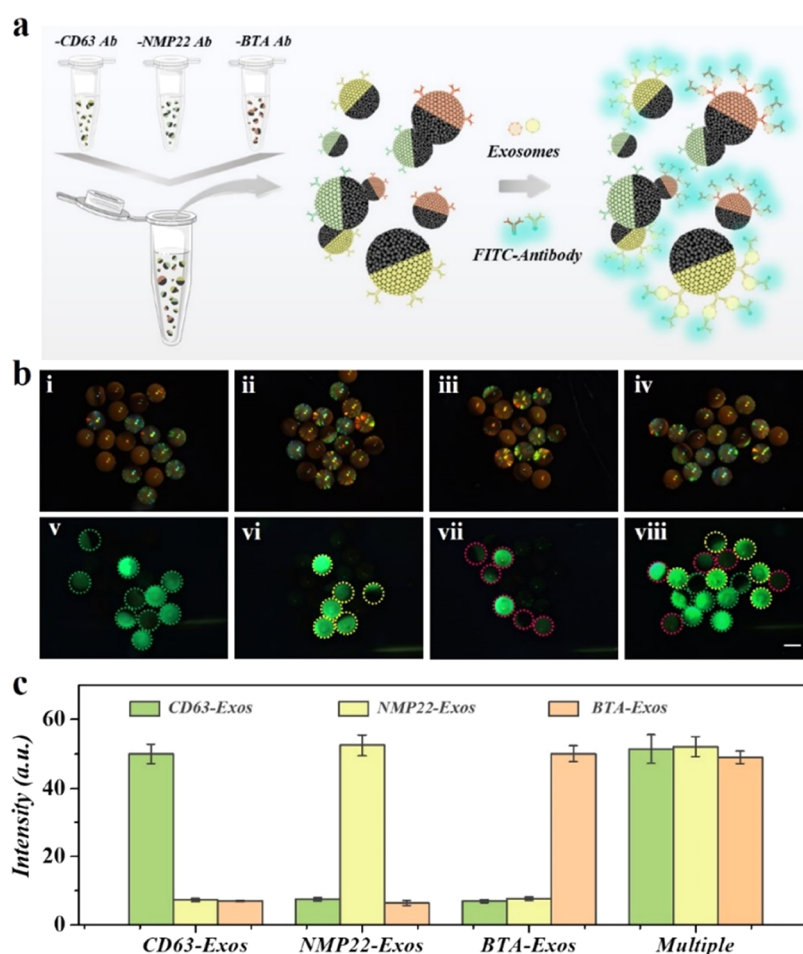


**Figure 4.** (a) Schematic diagram of the multiplexed platform for exosome analysis via the Janus magnetic microspheres. (b) (i–iv) Bright-field and the corresponding (v–viii) fluorescence microscopic images of three types of Janus magnetic microspheres after incubating with (i, v) CD63-exos, (ii, vi) NMP22-exos, (iii, vii) BTA-exos, and (iv, viii) the multiple exosomes. The scale bar is 400  $\mu\text{m}$ . (c) Fluorescence intensity analysis for Janus magnetic microspheres after incubating with CD63-exos, NMP22-exos, BTA-exos, and the multiple exosomes.

the capture of bladder cancer exosomes. CD63 is a general marker for the capture of exosomes. In addition, nuclear matrix protein 22 (NMP22) and bladder tumor-associated antigen (BTA), as the specific markers of bladder cancer-related exosomes, have been approved by the Food and Drug Administration (FDA) for clinical screening of bladder cancer.<sup>26</sup> Based on this, exosomes were extracted from human bladder cancer cells (T24) and human bladder epithelial immortal cells (sv-huc-1). Specifically, exosomes were extracted by ultracentrifugation from the cell culture medium. The biological characteristics of exosomes were analyzed from several aspects. The morphology was confirmed by transmission electron microscopy (TEM), as shown in Figure 3a. The exosomes showed the typical double-layer capsule-like structure after uranium acetate staining. The distribution of exosome particle size was measured through nanoparticle tracking analysis (NTA), and the average diameter of the exosomes was 74.39 nm (Figure 3b). The Western blot method was used to appraise the exosome specific markers, and the results showed that the exosome characteristic protein CD63 was expressed in both of cell-derived exosomes, and NMP22 and BTA were significantly expressed in the exosomes from bladder cancer cells but not in normal bladder epithelial cell exosomes (Figure 3c).

**3.3. Exosome Analysis Using Janus Magnetic Microspheres.** We designed a platform for quantitative analysis of bladder cancer exosomes based on the Janus magnetic microspheres. Specifically, the microspheres were first immobilized with CD63, NMP22, or BTA antibody probes after appropriate chemical modifications. Exosomes extracted by ultracentrifugation were prepared into standard samples of gradient concentration and were incubated with the microspheres. Thereafter, FITC-labeled detection antibodies participated in the reaction system to generate a double-binding complex for exosome detection. We found that the fluorescence intensity of the microspheres increased significantly with the increase of exosome concentration from  $10^3/\text{mL}$  to  $10^7/\text{mL}$ , indicating more exosomes being captured. Accordingly, we performed a correlation fitting between fluorescence intensity and the exosome concentration measured by CD63, as shown in Figure 3d. Similarly, the correlation measured by BTA and NMP22 is shown in Figure S8a,b, respectively.

We further optimized the experimental parameters for exosome capture and detection. It is worth mentioning that the  $\text{Fe}_3\text{O}_4$  nanoparticles utilized in the fabrication of the Janus magnetic microspheres were self-prepared by coprecipitation of ferrous chloride and ferric chloride. We thus explored the effect of  $\text{FeCl}_3$  concentration on exosome analysis of  $\text{Fe}_3\text{O}_4$

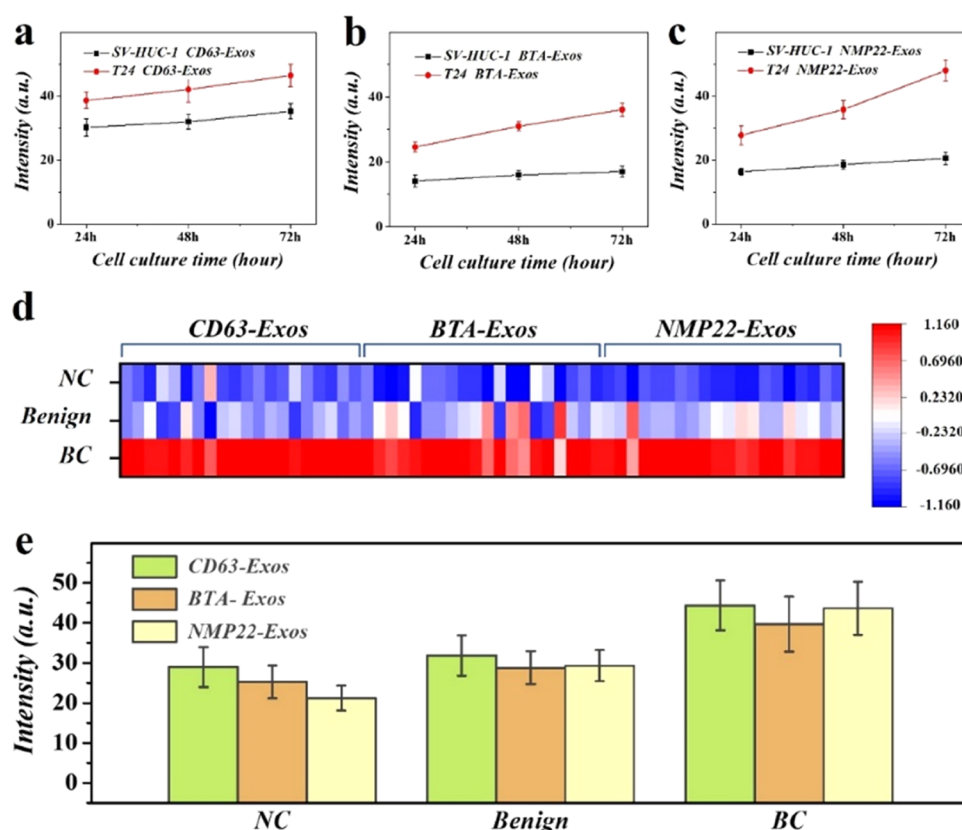


**Figure 5.** (a) Fluorescence intensity of the Janus magnetic microspheres incubates with exosomes extracted from T24 and sv-huc-1 cells at different timepoints of culture. The error bars represent the standard deviation of three repeated experiments. (b) Heat map analysis of the concentrations of urinary CD63-exos, NMP22-exos, and BTA-exos in the patients with bladder cancer, benign disease, and normal control (NC) group. (c–e) Fluorescence intensity analysis of CD63-exos, NMP22-exos, and BTA-exos in the urine of bladder cancer patients, benign disease, and NC group, respectively.

nanoparticle dispersion. After the comprehensive consideration, Janus barcodes with a  $\text{FeCl}_3$  concentration of 20 mg/mL had the acceptable detection signal intensity and appropriate mechanical properties, so we chose this concentration as the preparation condition of magnetic nanoparticles (Figure S9a). In addition, compared with classical uniform PhC microspheres, the Janus magnetic microspheres had an improved detection efficiency due to the magnetic-controllable motion (Figure S9b). This was probably attributed to enhanced contact between the probes and exosomes, indicating that the Janus magnetic microsphere could support low-sample-volume bioanalysis in complex systems. Meanwhile, we optimized the probe concentration and the reaction time. Five concentration gradients and six reaction time gradients were analyzed by the detection of the fluorescence intensity. The results showed that when the probe concentration was 0.01 mg/mL during the reaction time of 2 h, the detection signal of exosomes reached the saturation level (Figure S10a,b). Moreover, we validated the reliability of this platform by testing the exosome detection specificity. We prepared a coexisting system and measured the fluorescence intensity of a specific analyte by changing the concentration of other analytes. The results suggested that, as the concentration of an interfering analyte increased, the signal fluctuation amplitudes of the specific analytes were less than 5%, indicating that the multiplexed analysis platform had an ideal anti-interference and specificity (Figure S11).

#### 3.4. Multiplexed Analysis of Exosomes Based on Janus Magnetic Microspheres.

To realize multiplexed

analysis, the Janus magnetic microspheres with the reflection peaks of 565, 595, and 610 nm (in bright green, yellow-green, and orange-red colors, respectively) were selected to connect with Anti-CD63 antibody, anti-NMP22 antibody, and anti-BTA antibody, respectively. These probe-immobilized microspheres were incubated together with the bladder cancer exosome samples. Then, FITC-labeled anti-CD63, anti-NMP22, and anti-BTA were added to the detection solution, as illustrated in Figure 4a. After the reaction was completed, the Janus magnetic microspheres were characterized by fluorescence imaging (Figure S12). Based on the multiencoding principle of structural colors, fluorescence microscopy was utilized to analysis the characteristic spectra to decode the Janus barcodes (Figure 4b). Besides, a fluorescence spectrometer was used to detect the fluorescence signal of the encoding microcarriers, while the signal intensity quantified the exosomes (Figure 4c).

We analyzed the expression of markers for exosomes extracted at different timepoints of culture of the sv-huc-1 cells and T24 cells. The fluorescence intensity of the Janus magnetic microspheres after incubated with extracted exosomes was measured. The results showed that the expression of CD63, the general exosome marker, was higher in T24 cells than in sv-huc-1 cells, but it did not increase dramatically with the extension of cell culture time. However, the fluorescence intensity of NMP22 and BTA in T24 cells was significantly higher than that of sv-huc-1, and it increased observably with the extending of the culture time (Figure 5a).

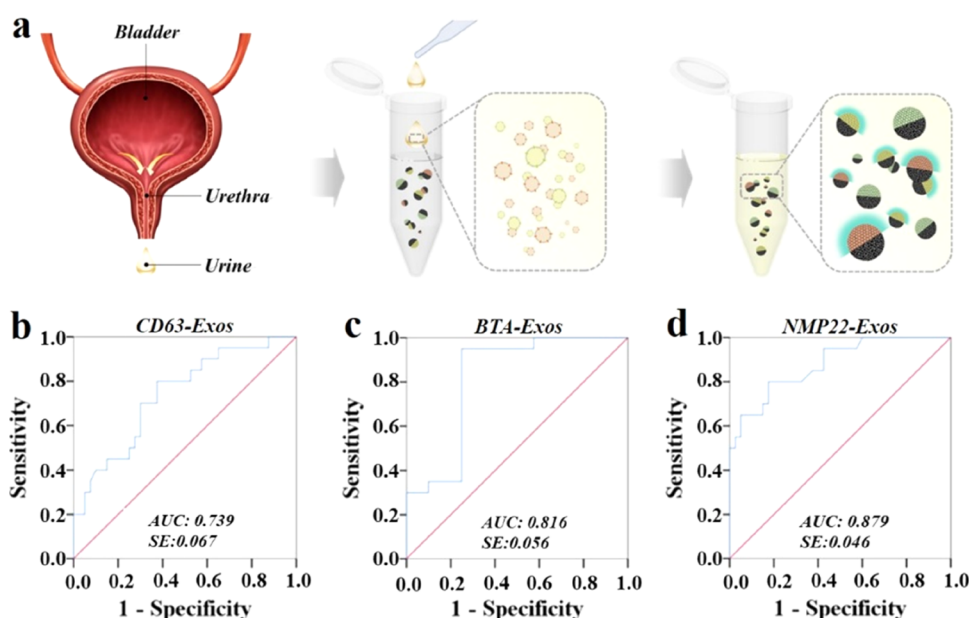


**Figure 6.** (a) Schematic diagram of the urine specimen analysis. (b–d) ROC curves of bladder cancer-derived exosomes were analyzed by the Janus magnetic microspheres. Each specimen was detected three times.

We further extended the application of this multiplexed platform to analyze urinary exosomes from the patients with bladder cancer and benign disease such as the bladder inflammation and benign bladder tumors in the Second Affiliated Hospital of Nanjing Medical University (Institutional Review Board Project No. [2021]-KY-061-01). Samples taken from healthy people were selected as the normal control (NC) (Table S1). Results indicated that the detection signal value of exosome markers in bladder cancer samples was significantly greater than that of benign disease and NC groups ( $p < 0.05$ ) (Figure 5b,c). Furthermore, the receiver operating characteristic (ROC) curve demonstrated the analytical sensitivity and specificity of bladder cancer-related exosomes. As a performance indicator of the detection system, the area under the curve (AUC) analysis results of CD63-exos, BTA-exos, and NMP22-exos were 0.739, 0.816, and 0.879, respectively (Figure 6b), predicting the potential utility of the novel multiplexed assay platform for bladder cancer-derived exosome detection and clinical diagnosis.

#### 4. CONCLUSIONS

In this research work, we constructed a multiplex analysis platform based on Janus magnetic microcarriers for the quantitative detection of bladder cancer exosomes. The Janus magnetic microcarriers were generated from microfluidic droplets containing colloidal silica nanoparticles and magnetic nanoparticles. Through droplet evaporation and magnetic-induced phase separation, the nanoparticles assembled into Janus microspheres with one hemisphere showing structural color and the other hemisphere showing magneto-responsiveness. The structural color constituted the encoding element of the microcarriers; meanwhile, the magneto-responsiveness feature made them capable of the controllable motion. The combination of these two features allowed the microcarriers to serve as barcodes for multiplex bioassays with high detection specificity and sensitivity. Based on this platform, we realize the multiplexed quantitative analysis of several bladder cancer-derived exosomes from the urine specimen with a small sample

volume as low as 20  $\mu\text{L}$ . The results demonstrated the excellent detection performance of this platform and indicated great potential in clinical diagnosis of exosome biomarkers and monitoring the development of bladder cancer.

#### ■ ASSOCIATED CONTENT

##### Supporting Information

The Supporting Information is available free of charge at <https://pubs.acs.org/doi/10.1021/acs.analchem.2c04408>.

Additional methods and experimental details including the statistical table of clinical specimen characteristics (PDF)

#### ■ AUTHOR INFORMATION

##### Corresponding Authors

**Luoran Shang** – Shanghai Xuhui Central Hospital, Zhongshan-Xuhui Hospital, and the Shanghai Key Laboratory of Medical Epigenetics, the International Co-Laboratory of Medical Epigenetics and Metabolism (Ministry of Science and Technology), Institutes of Biomedical Sciences, Fudan University, Shanghai 200032, China; [orcid.org/0000-0001-7458-9100](https://orcid.org/0000-0001-7458-9100); Email: [luoranshang@fudan.edu.cn](mailto:luoranshang@fudan.edu.cn)

**Yuanjin Zhao** – Department of Clinical Laboratory, Nanjing Drum Tower Hospital, School of Biological Science and Medical Engineering, Southeast University, Nanjing 210096, China; [orcid.org/0000-0001-9242-4000](https://orcid.org/0000-0001-9242-4000); Email: [yjzhao@seu.edu.cn](mailto:yjzhao@seu.edu.cn)

**Weijian Sun** – Department of Gastrointestinal Surgery, The Second Affiliated Hospital and Yuying Children's Hospital of Wenzhou Medical University, Wenzhou 325027, China; Email: [fame198288@126.com](mailto:fame198288@126.com)

##### Authors

**Xiaowei Wei** – Department of Gastrointestinal Surgery, The Second Affiliated Hospital and Yuying Children's Hospital of Wenzhou Medical University, Wenzhou 325027, China; Laboratory Medicine Center, The Second Affiliated Hospital



of Nanjing Medical University, Nanjing 210011, China;

orcid.org/0000-0003-2157-505X

**Lijun Cai** – Department of Clinical Laboratory, Nanjing Drum Tower Hospital, School of Biological Science and Medical Engineering, Southeast University, Nanjing 210096, China

**Hanxu Chen** – Department of Clinical Laboratory, Nanjing Drum Tower Hospital, School of Biological Science and Medical Engineering, Southeast University, Nanjing 210096, China; orcid.org/0000-0001-7656-023X

Complete contact information is available at:

<https://pubs.acs.org/10.1021/acs.analchem.2c04408>

## Author Contributions

L.R.S., Y.J.Z., and W.J.S. conceived the idea and designed the experiment. X.W.W., L.J.C., and H.X.C. conducted experiments and data analysis. X.W.W. and L.R.S. wrote the manuscript.

## Notes

The authors declare no competing financial interest.

## ACKNOWLEDGMENTS

This work was supported by the National Key Research and Development Program of China (2020YFA0908200), National Natural Science Foundation of China (52073060), Guangdong Basic and Applied Basic Research Foundation (2021B1515120054), Shenzhen Fundamental Research Program (JCYJ20190813152616459 and JCYJ20210324133214038), and Natural Science Foundation of Jiangsu (BK20220737).

## REFERENCES

- (1) Bray, F.; Ferlay, J.; Soerjomataram, I.; Siegel, R. L.; Torre, L. A.; Jemal, A. *Ca-Cancer J. Clin.* **2018**, *68*, 394–424.
- (2) Wild, C. P.; Weiderpass, E.; Stewart, B. W. *World Cancer Report: Cancer Research for Cancer Prevention*; WHO, 2020.
- (3) Grayson, M. *Nature* **2017**, *551*, S33.
- (4) Darling, D.; Luxmanan, C.; O'Sullivan, P.; Lough, T.; Suttie, J. *Adv. Ther.* **2017**, *34*, 1087–1096.
- (5) Dimashkieh, H.; Wolff, D. J.; Smith, T. M.; Houser, P. M.; Nietert, P. J.; Yang, J. *Cancer Cytopathol.* **2013**, *121*, 591–597.
- (6) Sharifuzzaman, M.; Barmann, S. C.; Zahed, M. A.; Sharma, S.; Yoon, H.; Nah, J. S.; Kim, H.; Park, J. Y. *Small* **2020**, *16*, No. e2002517.
- (7) Zhang, C.; Zhao, Y. M.; Xu, X. M.; Xu, R.; Li, H. W.; Teng, X. Y.; Du, Y. Z.; Miao, Y. Y.; Lin, H. C.; Han, D. *Nat. Nanotechnol.* **2020**, *15*, 709–715.
- (8) Masud, M. K.; Na, J.; Younus, M.; Hossain, M. S.; Bando, Y.; Shiddiky, M. J.; Yamauchi, Y. *Chem. Soc. Rev.* **2019**, *48*, 5717–5751.
- (9) Pan, S. J.; Zhang, Y.; Natalia, A.; Lim, C. Z.; Ho, N. R.; Chowbay, B.; Loh, T. P.; Tam, J. K.; Shao, H. L. *Nat. Nanotechnol.* **2021**, *16*, 734–742.
- (10) Urquidí, V.; Rosser, C. J.; Goodison, S. *Curr. Med. Chem.* **2012**, *19*, 23.
- (11) Satyal, U.; Srivastava, A.; Abbosh, P. H. *Front. Oncol.* **2019**, *9*, 1266.
- (12) Gutiérrez Baños; Banos, J.; Rebollo, R. M.; Antolin, J. F.; Martin, G. B. *Urol. Int.* **2001**, *66*, 185–190.
- (13) Li, W. Z.; Wang, H. Y.; Zhao, Z. J.; Gao, H. Q.; Liu, C. L.; Zhu, L.; Wang, C.; Yang, Y. L. *Adv. Mater.* **2019**, *31*, No. e1805344.
- (14) Xu, R.; Rai, A.; Chen, M.; Suwakulsiri, W.; Greening, D. W.; Simpson, R. J. *Nat. Rev. Clin. Oncol.* **2018**, *15*, 617–638.
- (15) Liu, C.; Xu, X.; Li, B.; Situ, B.; Pan, W.; Hu, Y.; An, T.; Yao, S.; Zheng, L. *Nano Lett.* **2018**, *18*, 4226–4232.
- (16) Nawaz, M.; Camussi, G.; Valadi, H.; Nazarenko, I.; Ekström, K.; Wang, X. Q.; Principe, S.; Shah, N.; Ashraf, N. M.; Fatima, F.; Neder, L.; Kislinder, T. *Nat. Rev. Urol.* **2014**, *11*, 688–701.
- (17) Junker, K.; Heinzelmann, J.; Beckham, C.; Ochiya, T.; Jenster, G. *Eur. Urol.* **2016**, *70*, 323–331.
- (18) Street, J. M.; Koritzinsky, E. H.; Glispie, D. M.; Star, R. A.; Yuen, P. S. *Adv. Clin. Chem.* **2017**, *78*, 103–122.
- (19) Di Meo, A.; Bartlett, J.; Cheng, Y. F.; Pasic, M. D.; Yousef George, M. *Mol. Cancer* **2017**, *16*, 80.
- (20) Tan, W. S.; Tan, W. P.; Tan, M. Y.; Pramit, K.; Dong, L.; Patricia, D.; Feber, A.; Kelly, J. D. *Cancer Treat. Rev.* **2018**, *69*, 39–52.
- (21) D'Costa, J. J.; Goldsmith, J. C.; Wilson, J. S.; Bryan, R. T.; Ward, D. G. *Bladder Cancer* **2016**, *2*, 301–317.
- (22) Xylinas, E.; Kluth, L. A.; Rieken, M.; Karakiewicz, P. I.; Lotan, Y.; Shariat, S. F. *Urol. Oncol.* **2014**, *32*, 222–229.
- (23) Shah, R.; Patel, T.; Freedman, J. E. *N. Engl. J. Med.* **2018**, *379*, 958–966.
- (24) van Niel, G.; D'Angelo, G.; Raposo, G. *Nat. Rev. Mol. Cell Biol.* **2018**, *19*, 213–228.
- (25) Huang, R. R.; He, L.; Xia, Y. Y.; Xu, H. P.; Liu, C.; Xie, H.; Wang, S.; Peng, L. J.; Liu, Y. F.; Liu, Y.; He, N. Y.; Li, Z. Y. *Small* **2019**, *15*, No. e1900735.
- (26) Liang, K.; Liu, F.; Fan, J.; Sun, D. L.; Liu, C.; Lyon, C. J.; Bernard, D. W.; Li, Y.; Yokoi, K.; Katz, M. H.; Koay, E. J.; Zhao, Z.; Hu, Y. *Nat. Biomed. Eng.* **2017**, *1*, 21.
- (27) Zhang, P.; He, M.; Zeng, Y. *Lab Chip* **2016**, *16*, 3033–3042.
- (28) Wu, M.; Ouyang, Y.; Wang, Z.; Zhang, R.; Huang, P. H.; Chen, C. Y.; Li, H.; Li, P.; Quinn, D.; Dao, M.; Suresh, S.; Sadosky, Y.; Huang, T. J. *Proc. Natl. Acad. Sci. U.S.A.* **2017**, *114*, 10584–10589.
- (29) Chen, H. X.; Bian, F. K.; Sun, L. Y.; Zhang, D. G.; Shang, L. R.; Zhao, Y. J. *Adv. Mater.* **2020**, *32*, No. e2005394.
- (30) Wan, Y.; Cheng, G.; Liu, X.; Hao, S. J.; Nisic, M.; Zhu, C. D.; Xia, Y. Q.; Li, W. Q.; Wang, Z. G.; Zhang, W. L.; Rice, S. J.; Sebastian, A.; Albert, I.; Belani, C. P.; Zheng, S. Y. *Nat. Biomed. Eng.* **2017**, *1*, 58.
- (31) Stöber, W.; Fink, A.; Bohn, E. *J. Colloid Interface Sci.* **1968**, *26*, 62–69.
- (32) Ming, M.; Zhang, Y.; Yu, W.; Shen, H. Y.; Gu, N. *Colloids Surf., A* **2003**, *212*, 219–226.
- (33) Wang, Y.; Shang, L. R.; Chen, G. P.; Sun, L. Y.; Zhang, X. X.; Zhao, Y. J. *Sci. Adv.* **2020**, *6*, No. eaax8258.
- (34) Chao, Y.; Mak, S. Y.; Rahman, S.; Zhu, S.; Shum, H. C. *Small* **2018**, *14*, No. 201802107.
- (35) Xu, W. J.; Li, Z. W.; Yin, Y. D. *Small* **2018**, *14*, No. 1801083.
- (36) Zhang, Y. S.; Khademhosseini, A. *Science* **2017**, *356*, No. eaaf3627.
- (37) Xu, H.; Liao, C.; Zuo, P.; Liu, Z.; Ye, B. C. *Anal. Chem.* **2018**, *90*, 13451–13458.
- (38) Wang, H.; Liu, Y. X.; Chen, Z. Y.; Sun, L. Y.; Zhao, Y. J. *Sci. Adv.* **2020**, *6*, No. eaay1438.
- (39) Shang, L. R.; Cheng, Y.; Zhao, Y. J. *Chem. Rev.* **2017**, *117*, 7964–8040.
- (40) Xu, Y. S.; Wang, H.; Chen, B. A.; Liu, H.; Zhao, Y. J. *Sci. China Mater.* **2019**, *62*, 289–324.
- (41) Wang, J.; Chen, G. P.; Zhao, Z.; Sun, L. Y.; Zou, M. H.; Ren, J. A.; Zhao, Y. J. *Sci. China Mater.* **2018**, *61*, 1314–1324.
- (42) Shao, C. M.; Liu, Y. X.; Chi, J. J.; Wang, J.; Zhao, Z.; Zhao, Y. J. *Research* **2019**, No. 9783793.
- (43) Fu, Q. Q.; Zhu, H. M.; Ge, J. P. *Adv. Funct. Mater.* **2018**, *28*, No. 1804628.
- (44) Choi, T. M.; Je, K.; Park, J. G.; Lee, G. H.; Kim, S. H. *Adv. Mater.* **2018**, *30*, No. 1803387.
- (45) Hou, J.; Li, M. Z.; Song, Y. L. *Angew. Chem., Int. Ed.* **2018**, *57*, 2544–2553.